Desalination and Water Treatment
www.deswater.com
doi: 10.5004/dwt.2023.29356

287 (2023) 139–154
March

Polyethyleneimine modified NH_2-MIL-101(Fe) with high adsorption capacity towards hexavalent chromium and copper ion from solution

Peifeng Yang, Xu Liu*, Shanshan Chen, Runping Han*

College of Chemistry, Zhengzhou University, Kexue Dadao #100, Zhengzhou, China 450001, emails: lxcod@zzu.edu.cn (X. Liu), rphan67@zzu.edu.cn (R. Han), 326105497@qq.com (P. Yang), 2503579590@qq.com (S. Chen)

Received 14 October 2022; Accepted 4 February 2023

ABSTRACT

Metal–organic frameworks have unique structural, physical, and chemical properties, such as large specific surface area, high porosity, good crystalline structure, and thermal stability, and are thus found in broad applications in the field of water treatment. In this study, the facile synthesis of polyethyleneimine modified NH_2-MIL-101(Fe) was performed in a single step, and the adsorption property toward hexavalent chromium and copper ions was carried out. MIL-101(Fe)@PEI (PEI – Polyethylenimine) has a higher adsorption capacity than NH_2-MIL-101(Fe), indicating the composite is potential as an efficient adsorbent. The maximum adsorption capacity was 339 $mg \cdot g^{-1}$ for Cr(VI) (pH 5.5) and 32.9 $mg \cdot g^{-1}$ for Cu(II) (pH 5.0) from experimental results at 293 K, respectively. The process is a homogeneous physical and chemical adsorption, such as y ion exchange, surface complexation, and electrostatic attraction. For both Cr(VI) and Cu(II) adsorption, there is spontaneity and increasing entropy. Freundlich model is best suitable to fit the equilibrium data while pseudo-second-order kinetic model and double constant model can describe the kinetics of Cr(VI) and Cu(II), respectively. There is good property of spent adsorbent for regeneration and reuse. MIL-101(Fe)@PEI is promising as adsorbent for removal of some pollutants.

Keywords: MIL-101(Fe)@PEI; Adsorption; Hexavalent chromium; Copper ion; Regeneration

1. Introduction

As the most precious resource for human survival, water resources are facing unprecedented challenges [1]. Rapid urbanization and industrialization have destroyed the natural balance of the ecosystem. The activities of textile [2], food [3], cosmetics, printing [4], pharmaceutical industries [5], among others, have resulted in the release of large volumes of toxic organic chemicals and some heavy metals such as mercury, chromium and copper, into water bodies, creating a pertinent environmental pollution problem that requires immediate attention.

Some heavy metals are essential trace elements in life activities and cofactors involved in various biological processes. However, some of these elements, such as cadmium, mercury, lead, and arsenic, are well-known environmental pollutants. Increased concentrations of these heavy metals in water bodies will inhibit biological growth and reduce the development process of marine ecosystems, which has an impact on geology, hydrology, and the biological cycle [6]. Chromium (Cr) exists in nature in two relatively stable oxidation states, namely Cr(III) and Cr(VI). Although the presence of Cr(VI) will interfere with the repair mechanism of cells and induce gene mutation, Cr(III) is generally considered less harmful than Cr(VI) [7]. Chromium-containing substances are some of the most toxic pollutants due to their high solubility and fluidity. In addition, Cr(VI) has a strong carcinogenicity, causing great harm to the human body. According to the US Environmental Protection Agency, the permissible limit of total chromium in drinking water

* Corresponding authors.

1944-3994/1944-3986 © 2023 Desalination Publications. All rights reserved.

is 0.1 mg·L^{-1}. Therefore, it is necessary to remove harmful Cr(VI) from wastewater before it is discharged into the environment. Copper (Cu) plays an important role in the metabolism of living systems and is a well-known micronutrient for plants and animals. However, a large intake of Cu and a lack of Cu in the body will also cause harm to the human body [8]. When copper accumulates in the body to a certain extent, it will cause harm to human health and can cause necrotizing hepatitis and haemolytic anaemia [9]. Unlike organic pollutants, heavy metals are toxic or carcinogenic. They are not biodegradable and can accumulate in living organisms. In order to prevent the carcinogenicity resulting from Cr and Cu compounds, it is very important to remove heavy metal pollutants from wastewater and meet the discharge standards.

Polyethylenimine (PEI) is a kind of high-density amine polymer with a primary amine active site at the chain end. The PEI chain has good biocompatibility and is water soluble. The high density of the amino group on the PEI chain indicates that it has good water solubility, which is conducive to the stretching of the graft carrier in aqueous solution [10]. Various advantages have made PEI widely used in environmental remediation [11–13].

There is a transition from the traditional porous adsorbent materials to the development and use of metal-organic scaffolds due to their improved characteristics. These characteristics include high crystallization rate, highly ordered diversified hierarchical structure, high surface area and porosity, adjustable pore size, surface modification, and recyclability, just to mention only a few [14,15]. Metal–organic frameworks (MOFs) are a unique type of crystalline and porous solid material constructed from metal nodes (metal ions or clusters) and functional organic ligands [14]. The performance of MOFs can be adjusted by selecting different metal ions and organic linkers to improve the selectivity of target pollutants. Iron has been used in much of the research because of its low cost, abundant geological reserves, and eco-friendliness in the fabrication of MOFs through solvothermal processes. The solvothermal method refers to the self-assembly of organic ligands and metal ions by heating mixed reactants such as trivalent metal salts, carboxylic acids, and auxiliary solvents [15]. Jang et al. [16] synthesized metal–organic framework MIL-100(Fe) by hydrothermal treatment for Rhodamine B (RB) removal from aqueous solutions. A magnetic MOF composite, MIL-101(Fe)@PDopa@Fe_3O_4, was synthesized as the stable adsorbent by Hamedi et al. [17] using the solvothermal method for removal of Methyl red (MR) and Malachite green (MG) from wastewaters. Yang et al. [18] used the solvothermal method to preparation of MIL-101COOH microcrystals adsorptive removal of anionic dyes. Arora et al. [19] facilely synthesized Fe-BDC by hydrothermal treatment to removal of methylene blue dye from industrial waste. Chen et al. [20] facilely synthesized MIL-100(Fe) by hydrothermal treatment, and MIL-100(Fe) was used as an adsorbent to remove neutral red (NR) from aqueous solution. Burtch et al. [21] inserted $H_3PMo_{12}O_{40}$ into MIL-100 (Fe) cavity through a hydrothermal process, and the results showed that the synthesized HPMO@MIL-100(Fe) nanocomposites were stable and could be used as a promising catalyst for the reduction of heavy metal ions. The higher photoactivity of the HPMO@MIL-100(Fe) can be attributed to the combined effect of enhanced light absorption intensity and the separation of photogenerated electron hole pairs. Liang et al. [22] also used the hydrothermal method to prepare magnetic $P_2W_{18}O_{62}$@Fe_3O_4/MIL-101(Fe) nanocomposites for the removal of organic dyes in aqueous solution. Experimental results show that this highly electronegative MOF has a high selective adsorption capacity for cationic dyes and exhibit high stability and recoverability without changing the structure. Literature is replete with evidence of iron's ability to form stable metal ligand complexes with inorganic metal ions or clusters [23–25].

Based on the above analysis, the purpose of this study is to use a polyethyleneimine modified NH_2-MIL-101(Fe) as an efficient MOF with improved adsorption performance towards Cr(VI) and Cu(II) from aqueous solution. There are many functional groups of amino from PEI on the surface of composite, which can effectively bind Cu(II) through complex and Cr(VI) through electrostatic attraction and hydrogen bond. The effect of several factors on adsorption was performed and the kinetic process and isotherm curves were fitted using relative adsorption models. Furthermore, the mechanism of adsorption and regeneration of spent adsorbent was performed.

2. Materials and methods

2.1. Reagents and chemicals

All reagents used in the experiment are analytically pure and can be used without further purification. The reagents used in the experiment are primarily $Fe(NO_3)_3·9H_2O$, aminoterephthalic acid, polyethyleneimine, N,N-dimethylformamide, hydrochloric acid, sodium hydroxide, sodium chloride, calcium chloride, magnesium chloride, anhydrous ethanol, and distilled water.

2.2. Preparation of NH_2-MIL-101(Fe)

The solvothermal method was selected to synthesize the MOF. To begin, in a 30 mL solution of N,N-dimethylformamide, 808 mg $Fe(NO_3)_3·9H_2O$ and 362 mg NH_2-H_2BDC were stirred and heated in a 60°C water bath until evenly mixed, the mixture was transferred to a PTFE reactor, heated at 150°C until the reaction was completed (15 h). The mixed solution was dried to evaporate the excess reaction solvent, and then filtered and washed with distilled water and anhydrous ethanol three times. After vacuum drying for 12 h, the target product MIL-101(Fe) was obtained.

2.3. Preparation of composites of MIL-101(Fe)@PEI

Metal salt and linkers were mixed in an N,N-dimethylformamide solution and heated at 60°C, then 505 mg of PEI was added to the solution and heated and stirred in the water bath for 1 h. After PEI was completely dissolved in the mixed solution, 2 mL of 5% glutaraldehyde was added to the solution drop by drop. One hour later, the mixed solution was transferred to the Teflon reactor and heated at 150°C for 15 h. MIL-100(Fe)@PEI (brown-yellow powder) is

obtained by following a treatment protocol similar to that of MIL-100(Fe). Fig. 1 shows a schematic representation of the synthesis process of MIL-100(Fe)@PEI.

2.4. Characterization

A scanning electron microscope (SEM, Su8020, China) was employed to observe the morphology and microstructures of the prepared MOFs. Using the Fourier-transform infrared spectrometer (FTIR, Nicolet iS50, USA), the chemical groups on surface of two materials are analyzed. X-ray diffraction was used to determine the skeleton structure of the material at an angle range of 2–30 (XRD, X'Pert Pro, Holland). The nitrogen adsorption–desorption ratio surface area analyzer Brunauer–Emmett–Teller (BET, ASAP 2420-4MP, USA) was used to analyze aperture distribution and specific surface area. The absorption spectrum of Cr(VI) and Cu(II) was measured using an atomic absorption spectrophotometer (AAS, AA-7020, China). The isoelectric point of the material was measured by the 0.010 mol·L^{-1} NaCl solution addition method. A 10 mL solution was transferred into a series of 50 mL conical bottles, and the pH of the solution was adjusted to 2–11 using drops of HCl and NaOH. An amount of 0.010 g of the produced MOF material was added to the solution. After oscillating for 12 h at a constant temperature in a water bath at 303 K, they were separated by centrifugation. The pH value of the NaCl solution in the supernatant was determined, and the pH change was calculated, and a graph of pH against change in pH was plotted to determine the point of zero charge (pH_{pzc}) of the MOF.

2.5. Adsorption of Cr(VI) and Cu(II) from aqueous solution by MIL-101(Fe)@PEI

The adsorption capacity of MIL-101(Fe)@PEI toward heavy metals from solution was evaluated using Cr(VI) and Cu(II). To achieve adsorption equilibrium, 10 mg of adsorbent was added to 10 mL of Cr(VI) or Cu(II) solution with an initial concentration of 200 mg·L^{-1}, and the samples were oscillated for various periods at 303 K using at 120 rpm in a temperature-controlled orbital vibrator (SHA-82A, China). With the help of 0.1 mol·L^{-1} HCl and 0.1 mol·L^{-1} NaOH, the pH of Cr(VI) was adjusted from 2 to 12, and the pH of Cu(II) from 2 to 5.5. At 293, 303, and 313 K, the kinetics of Cr(VI) (initial concentration of 300 mg·L^{-1}) and Cu(II) (initial solution of 80 mg·L^{-1}) were investigated. At 293, 303, and 313 K, the equilibrium of Cr(VI) solution with an initial concentration of 50–600 mg·L^{-1} and Cu(II) solution with an initial concentration of 10–200 mg·L^{-1} was studied. After adsorption, the mixtures were centrifuged to determine the residual concentrations of Cr(VI) and Cu(II) in the solutions using atomic absorption spectroscopy (AAS). The adsorption capacity (q, mg·g^{-1}) of Cr(VI) and Cu(II) can be calculated by using the concentration difference before and after adsorption [Eq. (1)].

$$q_e = \frac{C_0 - C_e}{m} V \tag{1}$$

where C_0 is the initial NR concentration (mg·L^{-1}), C_e is the NR concentration at any time (t) or equilibrium (mg·L^{-1}), V is the NR solution volume (L), and m is the mass of MIL-100(Fe) (g).

The experiments were repeated twice, and the mean values were recorded and further used for the data analysis. The errors are less than 5%.

2.6. Reusability of the MOF

The spent adsorbents were obtained at following conditions: initial concentration 300 mg·L^{-1} for Cr(VI) and 120 mg·L^{-1} for Cu(II), temperature 303 K, solution volume 10 mL, dose 10 mg and contact time 200 min. Then spent adsorbents were separated by centrifugation and washed using distilled water. Then Cr-loaded adsorbent and the Cu-loaded adsorbent were regenerated using various solutions, respectively, followed by centrifugal separation and dried in hot air oven at 60°C. This adsorbent was again used for the removal of Cr(VI) and Cu(II) from aqueous solution. After each run, Cr(VI) and Cu(II) concentration in solution was determined. The recyclable MOF was reused for Cr(VI) and Cu(II) adsorption three times.

3. Results and discussion

3.1. Characterization of materials

3.1.1. Analysis of zero point charge (pH_{zpc}) of MIL-101(Fe)@PE

The isoelectric points of the synthesized materials are shown in Fig. 2a. It was observed that after PEI was

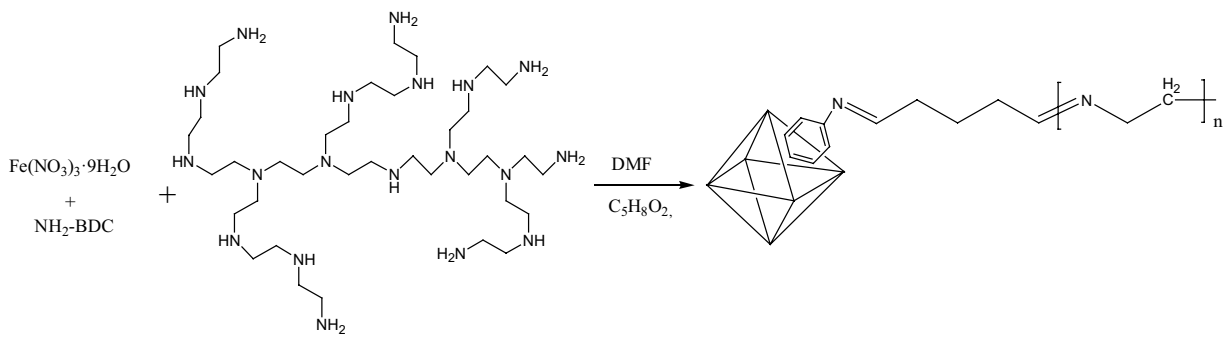

Fig. 1. Synthesis process of NH_2-MIL-101(Fe) and MIL-101(Fe)@PEI.

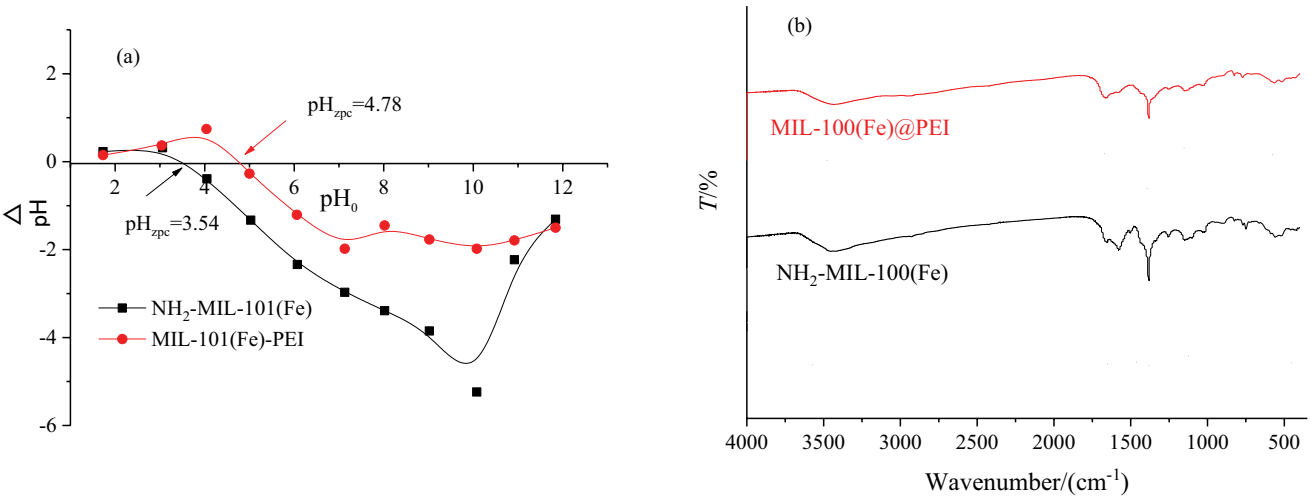

Fig. 2. (a) Isoelectric point diagram of the materials and (b) FTIR of NH_2-MIL-101(Fe) and MIL-101(Fe)@PEI.

cross-linked to the surface of NH_2-MIL-101(Fe), the pH_{zpc} of the NH_2-MIL-101(Fe) increased from 3.54 to 4.78, indicating that the addition of PEI increased the base groups on the surface of MIL-101(Fe)@PEI. This is explained by the fact that the surface charge of an adsorbent is affected by pH through the dissociation of functional groups on the active sites of the adsorbent as well as the solution dye chemistry [13]. Similar observations have been reported in literature by Kani et al. [13].

3.1.2. FTIR analysis

FTIR spectrum analysis is an important tool for characterising covalent and non-covalent functional groups and can be used to validate material surface functionalization. To verify the changes of surface functional groups before and after modification, infrared spectrum analysis was performed on NH_2-MIL-101(Fe) and MIL-101(Fe)@PEI, and the results are shown in Fig. 2b.

As can be seen from Fig. 2b, the wide peak around 3,450 cm^{-1} is attributed to the joint action of –OH group and $–NH_2$ groups. The wide absorption peak at about 3,442 cm^{-1} is the stretching vibration of –OH group, and the peak at 1,618 cm^{-1} is generated by the skeleton vibration of benzene ring. The absorption peak at 1,450 cm^{-1} is due to the existence of C=C stretching vibration. The peak at 1,373 cm^{-1} may be the stretching vibration of $–CH_3$. The band at 1,315 cm^{-1} is attributed to C–O stretching vibration, and the absorption peak at 548 cm^{-1} is associated with the Fe–O bond, which suggests that the Fe^{3+} has successfully reacted with the carboxylic acid group and produced a new chemical bond. The slight shift in peak position and the decrease in peak intensity in some of the bands could be due to the interactions among the functional groups during the NH_2-MIL-101(Fe) and MIL-101(Fe)@PEI.

3.1.3. XRD analysis

XRD analysis is one of the important analysis methods in the qualitative and quantitative study of samples. Fig. 3 shows the comparison between the XRD spectra of NH_2-MIL-101(Fe) and MIL-101(Fe)@PEI and the standard spectra. As shown in Fig. 3, the XRD patterns of NH_2-MIL-101(Fe) prepared by the solvothermal method show three characteristic peaks at about 10°, 17° and 19°, indicating the successful preparation of NH_2-MIL-101(Fe). The disappearance of some peaks and the reduction in intensities of others may be due to the reduction of free body cavities in the material caused by the addition of PEI, resulting in a change in the structure of the MIL-101(Fe)@PEI.

3.1.4. BET analysis

The adsorption capacity of adsorbents is significantly affected by morphological parameters such as pore size, surface area, and total porosity. The N_2 adsorption–desorption isotherm analysis of the Barrett–Joyner–Halenda (BJH) model is commonly used to explain the porous structure of materials. This analysis provides information on porosity, pore-size distribution, porous material, and specific surface area. The N_2 adsorption–desorption isotherms of the two materials are shown in Fig. 4(left). As can be seen from Fig. 4, both adsorption–desorption isotherms fit well with the Type I isotherms defined by the International Society for Theoretical and Applied Chemistry, and type I isotherms are usually used to explain the presence of microporous structures or single-layer physical adsorption processes in materials. Both materials have adsorption isotherms characteristic of an almost horizontally parallel H_4 hysteresis ring, attributed to having narrow slits.

The pore-size distribution helps to determine the fraction of the total pore volume available for a molecule of a given size and shape. Fig. 4(right) shows the pore-size distribution of the adsorbent materials, and the results are listed in Table 1. The average pore sizes of the adsorbent materials are in the range of 2~50 nm, which indicates that the adsorbent materials are all mesoporous materials. The microporous area occupies half of the material surface area, indicating that microporous and mesoporous coexist in the adsorbents.

Compared with NH_2-MIL-101(Fe), the specific surface area of MIL-101(Fe)@PEI is reduced to 1.90 $m^2 \cdot g^{-1}$, which may be caused by the blockage of some pores by the cross-linked PEI on the surface of NH_2-MIL-101(Fe). The cross-linked functional groups on the surface of the material will lead to a decrease in pore size, suggesting a steric hindrance inhibiting the adsorption of N_2 molecules.

3.1.5. SEM analysis

SEM analysis is used to detect the surface morphology of the material, which can reflect the true image of the cross section in a single sample, and obtain direct information about the pore size, true pore shape and pore connectivity. In order to make the SEM analysis results representative of the whole sample, a large number of images should be taken at different positions of the sample. Fig. 5 shows the SEM characterization results of the cross sections of the powders of NH_2-MIL-101(Fe) and MIL-101(Fe)@PEI.

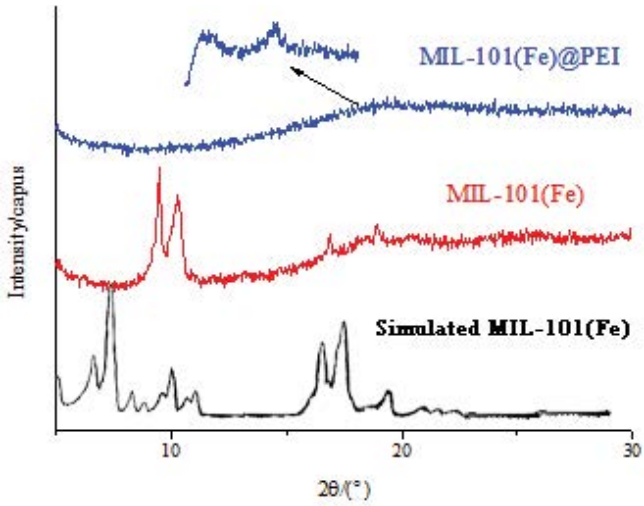

Fig. 3. X-ray diffraction of NH_2-MIL-101(Fe) and MIL-100(Fe)@PEI.

SEM analysis is used to visualize the true image of the cross section of a material and obtain some information on the pore size, the shape of the pore, and pore connectivity. To make the SEM analysis results representative of the whole sample, several images were taken at different positions on the material. The SEM images of the cross sections of the powders of NH_2-MIL-101(Fe) and MIL-101(Fe)@PEI are shown in Fig. 5.

As can be seen from Fig. 5, by comparing the surface morphology of NH_2-MIL-101(Fe) and MIL-101(Fe)@PEI, NH_2-MIL-101(Fe) is stacked by small particles with irregular shapes, and the material has more voids. After PEI cross-linking, the surface of NH_2-MIL-101(Fe) becomes smooth, the growth density increases, the slit decreases, and the surface becomes smoother. This is in line with the reduction in pore sizes seen in the BET analysis.

3.2. Adsorption study

3.2.1. Effect of pH on adsorption

The pH of the solution can change the surface charge of the adsorbent, resulting in the conversion of chromium ions in the solution and influencing the degree of dissociation of functional groups at the active site of the MIL-101(Fe)@PEI adsorbent. The adsorption of Cr(VI) and Cu(II) by MIL-101(Fe)@PEI under different pH conditions is shown in Fig. 6.

The amino groups on the surface of MIL-101(Fe)@PEI are easily protonated, resulting in an increase in the number of active sites. At a solution pH < 2, Cr(VI) mainly exists in the form of H_2CrO_4, and at pH between 2–6.8, Cr(VI) exists in the form of $HCrO_4^-$ and $Cr_2O_7^{2-}$. At pH > 6.8, Cr(VI) exists in the form of CrO_4^{2-}. Therefore, the negative potentials of $HCrO_4^-$, $Cr_2O_7^{2-}$ and CrO_4^{2-} are enhanced successively with the increase of solution pH.

MIL-101(Fe)@PEI has a higher adsorption capacity for Cr(VI) under acidic conditions than under alkaline conditions, as shown in Fig. 6. This could be due to the positive charged surface of the adsorbent at pH below pH_{zpc} of 4.78, resulting in a strong electrostatic attraction between

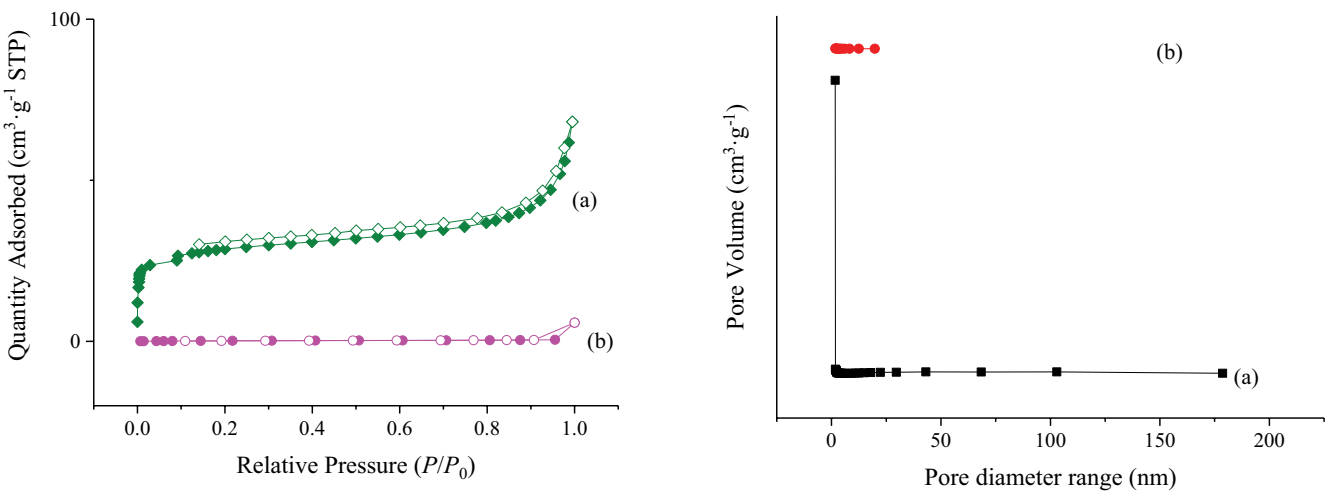

Fig. 4. N_2 adsorption–desorption curve (left) and pore-size distribution (right) of (a) NH_2-MIL-101(Fe) and (b) MIL-101(Fe)@PEI.

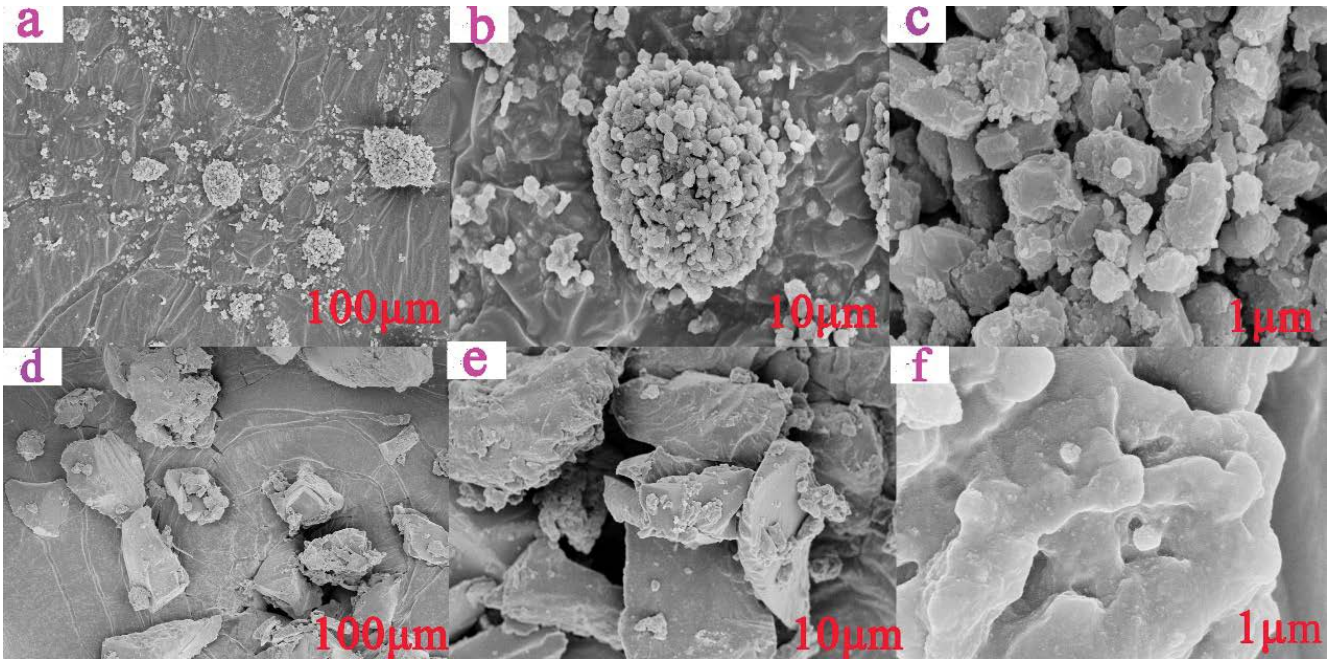

Fig. 5. Scanning electron microscope images of NH_2-MIL-101(Fe) (a–c) and MIL-101(Fe)@PEI (d–f).

Table 1
Specific surface area and pore size of materials before and after modification

Parameters	NH_2-MIL-101(Fe)	MIL-101(Fe)@PEI
Brunauer–Emmett–Teller surface area ($m^2 \cdot g^{-1}$)	103.7	1.90
Micropore volume ($cm^3 \cdot g^{-1}$)	0.0222	0.00091
Micropore area ($m^2 \cdot g^{-1}$)	58.2	0.476
Total pore volume ($cm^3 \cdot g^{-1}$)	0.105	0.0039
Average pore size (nm)	4.06	3.20

the ions in solution and the charged surface of the adsorbent. This explains the high adsorption capacity in acidic mediums. The electrostatic repulsion of chromium ions and the positively charged MIL-101(Fe)@PEI surface could explain the reduced adsorption capacity in alkaline medium. This observation is consistent with the report by Han et al. [26]. The potassium dichromate solution has an unadjusted pH of around 5.5, and MIL-101(Fe)@PEI demonstrated a high adsorption capacity for Cr(VI) under this condition. Adsorption data was subsequently collected at the potassium dichromate solution's initial pH without any adjustment.

According to Fig. 6, the adsorption capacity of MIL-101(Fe)@PEI towards Cu(II) was from 3.12 $mg \cdot g^{-1}$ at pH 3 to 35.8 $mg \cdot g^{-1}$ at 6.0. This can be explained by the large positive charge due to amino protonation on the surface of MIL-101(Fe)@PEI within the pH range of 2–4.78, which results in electrostatic repulsion with Cu(II). Furthermore, the high concentration of H^+ in an acidic medium obstructs the interaction between ligand and Cu^{2+} and reduces the adsorption of Cu(II). With a gradual increase in solution pH, the electrostatic repulsion gradually decreases, favoring an increasing adsorption of Cu(II). It is posited that the surface of the MIL-101(Fe)@PEI becomes negative at pH greater than 4.78, which explains the existence of electrostatic attraction mediating the removal of Cu(II). The initial pH of the $Cu(NO_3)_2$ solution is 5.0, and floc formation is observed at pH 5.5, so the solution pH was not adjusted for the adsorption experiments on Cu(II).

3.2.2. *Effect of coexisted ions on adsorption*

Since wastewater contains common salts, it is necessary to investigate the influence of salt concentrations on sorption. As shown in Fig. 7, the adsorption capacity of MIL-101(Fe)@PEI towards Cr(VI) decreased as the concentration of coexisting ions increased, and the negative effect of Na_2SO_4 on Cr(VI) adsorption was twice as great as that of NaCl. This could be due to the large charge density of Na_2SO_4. The negative effect of coexisting ions on Cr(VI) adsorption confirms electrostatic attraction and/or ion exchange as the primary determinant of the adsorption process.

As seen in Fig. 7, coexisting ions have minimal influence on MIL-101(Fe)@PEI's adsorption capability towards Cu(II). This shows that ion exchange or electrostatic attraction are unlikely to be the primary causes of Cu(II) adsorption.

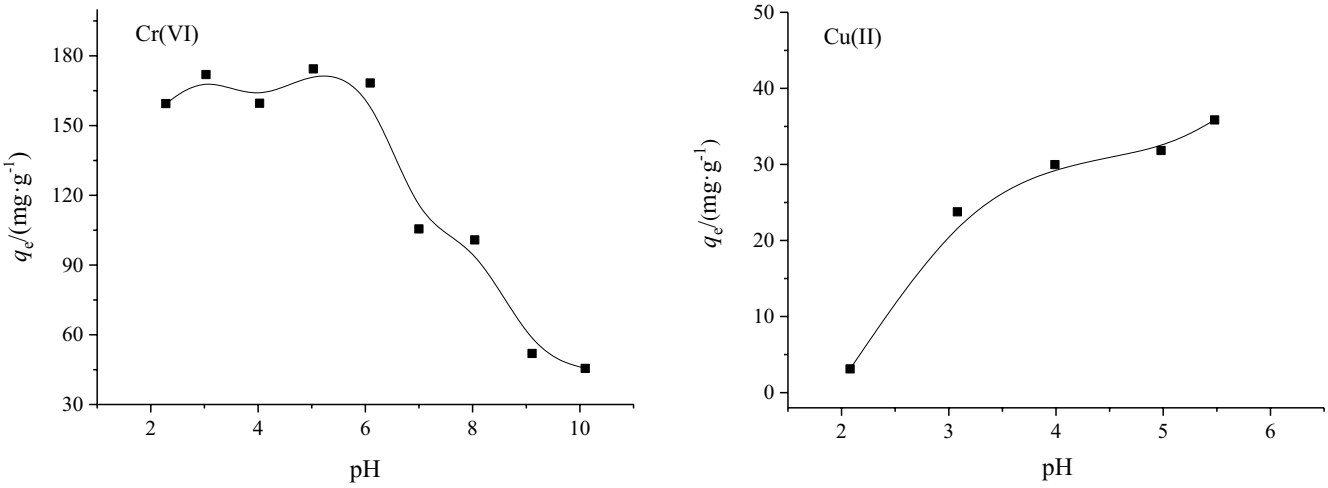

Fig. 6. Effect of pH on adsorption of Cr(VI) and Cu(II).

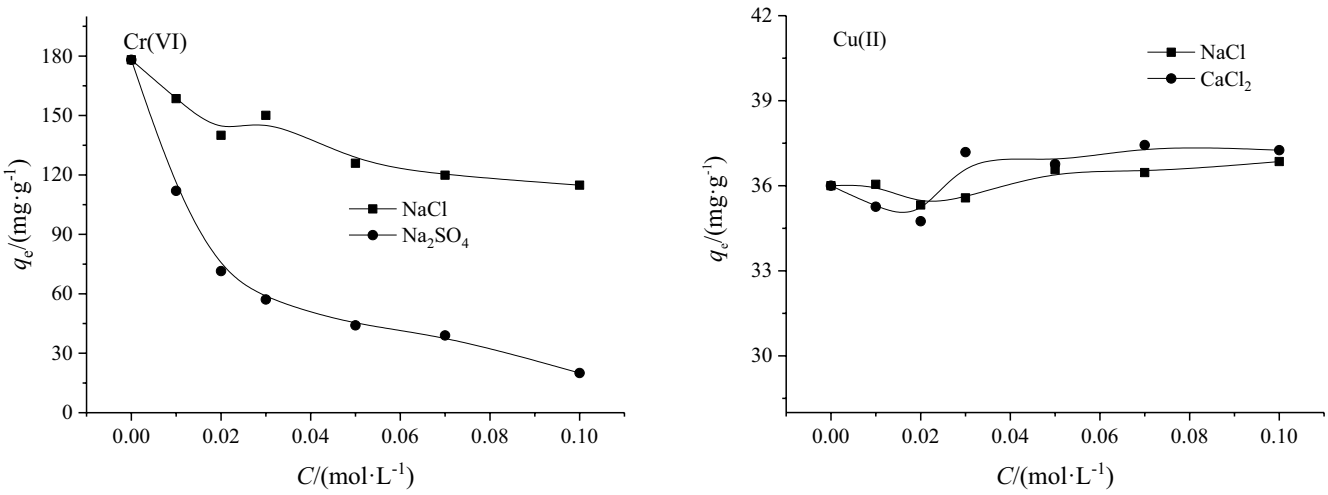

Fig. 7. Influence of co-existing ions on adsorption of Cr(VI) and Cu(II).

As a consequence, the adsorption process is suggested to be explained by complexation between MIL-101(Fe)@PEI and Cu(II).

3.2.3. Effect of adsorbent dosage on adsorption of Cr(VI) and Cu(II)

The results of the effect of dosage on adsorption are shown in Fig. 8. As shown in Fig. 8, the adsorption capacity (q_e) of MIL-101(Fe)@PEI for Cr(VI) and Cu(II) is inversely proportional to the removal rate (p), implying that adsorbate removal efficiency increases gradually as the mass of MIL-101(Fe)@PEI increases. This is because as the mass of the adsorbent is increased, there is a direct increase in the available active sites adsorbing the same amount of Cr(VI) and Cu(II) ions in solution, hence a reduction in the adsorption capacity. Subsequently, 0.010 g was selected as the optimal dosage of MIL-101(Fe)@PEI for Cr(VI) and Cu(II) in batch experiments.

The values of q_e of NH_2-MIL-101(Fe) toward Cr(VI) and Cu(II) were 65.4 and 24.3 mg·g^{-1}, respectively, at an initial concentration (C_0) of 200 mg·L^{-1} and a dose of 1.0 g·L^{-1}. At same conditions, the values of q_e of MIL(Fe)@PEI were 182 mg·g^{-1} for Cr(VI) and 39.2 mg·g^{-1} for Cu(II). This showed that the introduction of PEI significantly enhanced the adsorption capacity of NH_2-MIL-101(Fe) and the modification was valuable.

3.2.4. Effect of equilibrium concentration on adsorption

The concentration of Cr(VI) and Cu(II) in the solution at equilibrium was plotted against adsorption capacity (q_e), and the results are shown in Fig. 9. The adsorption capacity of MIL-101(Fe)@PEI for Cr(VI) decreased slightly with increasing temperature, indicating that the adsorption process was exothermic, as shown in Fig. 9. However, temperature was seen to have a weak influence on the adsorption of Cr(VI).

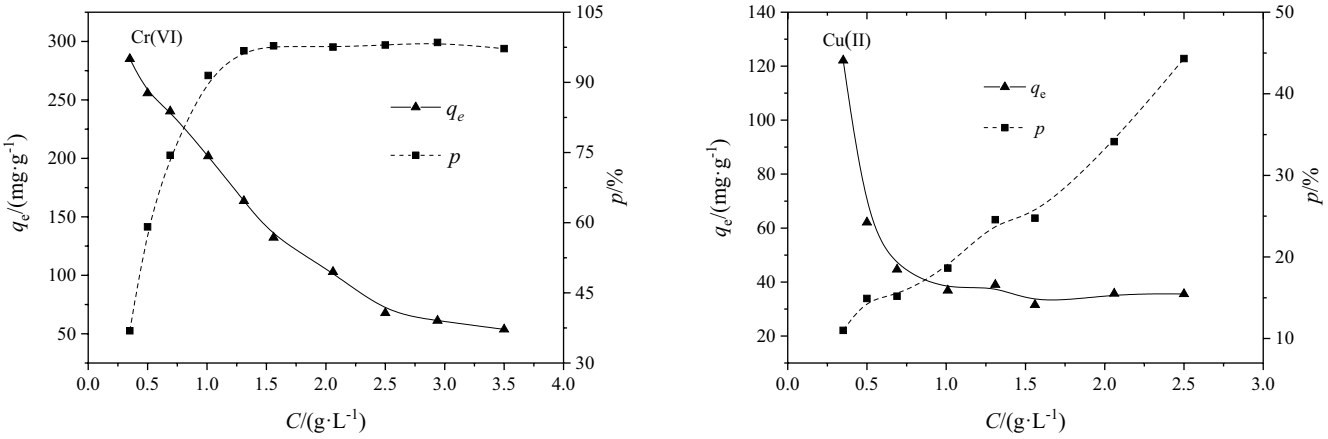

Fig. 8. Influence of adsorbent dosage on adsorption of Cr(VI) and Cu(II).

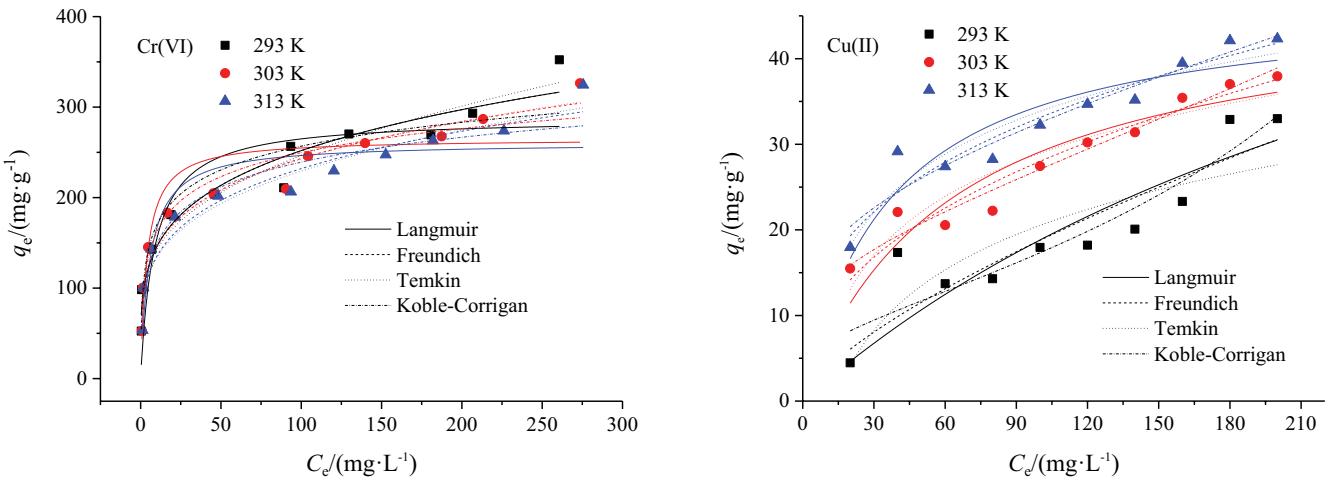

Fig. 9. Influence of concentration and temperature on adsorption of Cr(VI) and Cu(II) and the fitting curves.

According to Fig. 9, as the equilibrium concentration increases, Cu(II) adsorption on MIL-101(Fe)@PEI increases from 32.9 to 42.3 mg·g^{-1}. This is because increasing the adsorbate solution concentration increases the concentration gradient driving force, which accelerates Cu(II) diffusion to the adsorbent surface and reduces adsorption resistance, thereby increasing adsorption capacity. The adsorption capacity of MIL-101(Fe)@PEI for Cu(II) tends to increase with increasing temperature, indicating that an endothermic reaction occurs during the adsorption process.

Adsorption isotherm models have been used to describe the distribution of adsorbed molecules on the adsorbents after reaching an equilibrium state. Four isotherm models were used to describe the adsorption capacity of MIL-101(Fe)@PEI towards Cr(VI) and Cu(II). The expressions of the Langmuir model [Eq. (2)], the Freundlich model [Eq. (3)], the Koble–Corrigan model [Eq. (4)] and the Temkin model [Eq. (5)] are as follows:

$$q_e = \frac{q_m K_L C_e}{1 + K_L C_e} \tag{2}$$

$$q_e = K_F C_e^{1/n} \tag{3}$$

$$q_e = \frac{A C_e^n}{1 + B C_e^n} \tag{4}$$

$$q_e = A + B \ln C_e \tag{5}$$

where q_e (mg·g^{-1}) and q_m (mg·g^{-1}) are the maximum adsorption capacity and the equilibrium adsorption capacity, respectively; K_L (L·mg^{-1}) is a constant related to affinity of binding site and adsorption energy; C_e (mg·L^{-1}) is the concentration of adsorbent in equilibrium state; K_F is constant of Freundlich isotherm; $1/n$ is constant related to adsorption capacity and adsorption strength, and A and B are both constants of Temkin isotherm.

As can be seen from the fitting parameters in Table 2a, the adsorption quantity q_m obtained by the Langmuir model is significantly different from the experimental value q_m, with R^2 values ranging from 0.751 to 0.825. The fitted results according to the nonlinear regressive analysis are displayed in Table 2a, whereas Fig. 9 shows the fitted curves to the

Table 2a
Adsorption isotherm fitting parameters of MIL-101(Fe)@PEI for Cr(VI)

Langmuir					
T (K)	K_L (L·mg^{-1})	$q_{m(\exp)}$ (mg·g^{-1})	q_m (mg·g^{-1})	R^2	SSE
293	0.114 ± 0.061	339	287 ± 23.3	0.751	1.76 × 10^4
303	0.249 ± 0.097	326	265 ± 14.6	0.825	1.07 × 10^4
313	0.174 ± 0.068	324	260 ± 15.2	0.816	1.04 × 10^4
Freundlich					
T (K)	K_F	$1/n$	R^2	SSE	
293	84.0 ± 10.2	0.238 ± 0.025	0.943	4.03 × 10^3	
303	87.3 ± 9.21	0.222 ± 0.021	0.946	3.27 × 10^3	
313	78.2 ± 9.44	0.236 ± 0.025	0.938	3.51 × 10^3	
Temkin					
T (K)	A	B	R^2	SSE	
293	86.1 ± 16.2	37.9 ± 4.01	0.898	7.22 × 10^3	
303	73.1 ± 12.3	38.3 ± 3.05	0.940	3.67 × 10^3	
313	57.1 ± 14.4	39.5 ± 3.51	0.926	4.18 × 10^3	
Koble–Corrigan					
T (K)	A	B	n	R^2	SSE
293	63.9 ± 34.2	–0.296 ± 0.443	0.127 ± 0.121	0.942	3.64 × 10^3
303	85.4 ± 19.2	–0.031 ± 0.284	0.208 ± 0.127	0.939	3.27 × 10^3
313	71.2 ± 23.4	–0.132 ± 0.146	0.176 ± 0.146	0.931	3.47 × 10^3

$\mathrm{SSE} = \sum_{i=1}^{n}\left(q_c - q_e\right)^2$

experimental data. Based on the determined coefficients (R^2) and sum of square error (SSE) values, the Koble–Corrigan and Freundlich models are best to describe the equilibrium adsorption of Cr(VI) onto MIL-101(Fe)@PEI. However, Koble–Corrigan fitting is only valid when the constant "n" is greater than or equal to 1. From the data in Table 2a, it is suggested that Koble–Corrigan be incapable of defining the experimental data. Hence, the Freundlich model is the best fit to the equilibrium data, indicating the adsorption processes occur on heterogonous surfaces.

According to the fitting results listed in Table 2b, Freundlich model appears to best describe the experimental data of Cu(II) adsorption because it records the highest R^2 and the lowest SSE values. The deviation of n from unity ($1/n < 1$) indicates a nonlinear adsorption that takes place on heterogeneous surfaces. This behavior implies that the adsorption energy barrier increases exponentially as the fraction of occupied sites on MIL-101(Fe)@PEI increases.

Table 3 lists the comparison of the adsorption capacities of different adsorbents towards Cr(VI) and Cu(II). Despite the fact that many factors such as solution pH, concentration, and temperature influence adsorption capacity, MIL-101(Fe)@PEI has a promising application prospect for the removal of Cr(VI) and Cu(II) in solution due to its higher adsorption capacity. There are some competitive and advantage in application of the composite for removal of some organic pollutants.

Compared the values of q_e from experiments, there is higher adsorption capacity toward Cr(VI). This is due to the different mechanism Cr(VI) and Cu(II) binding. There are several ways about MIL-101(Fe)@PEI to bind Cr(VI), such as electronic attraction or ion-exchange, hydrogen bonding, etc. But for Cu(II) adsorption, surface complexation is major role of action. One copper ion can bind several nitrogen atoms from PEI. So the adsorption capacity toward Cu(II) is lower.

3.2.5. Adsorption kinetic study

Adsorption kinetics is an important factor which is crucial in understanding the adsorption process and the adsorbent performance as it reflects the rate of adsorption and the time required to reach equilibrium. The results of the kinetic study are presented in Fig. 10.

According to the kinetic results shown in Fig. 10, increasing the contact time increased the adsorption capacity of MIL-101(Fe)@PEI for Cr(VI) until equilibrium was reached, and the equilibrium time varied slightly depending on the temperature.

While the amount of Cr(VI) adsorbed onto a unit mass of MIL-101(Fe)@PEI was found to vary with temperature as a decrease in q_e was recorded with a rise in initial temperature, corroborating the exothermic nature of the adsorption process, the adsorption of Cu(II) onto MIL-101(Fe)@PEI saw an increase in q_e as temperature was increased from 293 to 313 K suggesting an endothermic process.

Five kinetic models were fitted to the experimental data, pseudo-first-order kinetic model [Eq. (6)], and

Table 2b
Adsorption isotherm fitting parameters of MIL-101(Fe)@PEI for Cu(II)

Langmuir					
T (K)	K_L (L·mg^{-1})	$q_{m(\exp)}$ (mg·g^{-1})	q_m (mg·g^{-1})	R^2	SSE
293	0.003 ± 0.002	32.9	40.3 ± 51.4	0.753	140
303	0.015 ± 0.004	37.9	47.4 ± 5.04	0.853	69.3
313	0.027 ± 0.001	42.3	47.1 ± 3.36	0.845	70.6
Freundlich					
T (K)	K_F	$1/n$	R^2	SSE	
293	0.73 ± 0.52	0.702 ± 0.141	0.958	120	
303	3.97 ± 0.79	0.424 ± 0.041	0.936	49.8	
313	78.2 ± 9.44	0.335 ± 0.038	0.913	39.7	
Temkin					
T (K)	A	B	R^2	SSE	
293	–26.4 ± 9.54	10.2 ± 2.19	0.816	169	
303	–16.6 ± 5.61	9.89 ± 1.23	0.876	58.6	
313	–11.3 ± 5.16	9.81 ± 1.13	0.891	49.6	
Koble–Corrigan					
T (K)	A	B	n	R^2	SSE
293	0.27 ± 0.03	–0.296 ± 0.443	$1.10 \times 10^{-7} \pm 8.59 \times 10^{-8}$	0.928	89.4
303	0.01 ± 0.42	–1.237 ± 27.66	$1.24 \times 10^{-7} \pm 1.21 \times 10^{-8}$	0.951	40.3
313	4.57 ± 50.1	–0.592 ± 4.901	0.067 ± 0.958	0.907	36.9

Table 3
Comparison of Cr(VI) and Cu(II) adsorption capacities of different adsorbent materials

Cr(VI)	q_m (mg·g^{-1})	References	Cu(II)	q_m (mg·g^{-1})	References
UFB-PPy	86.5	[27]	SDBS@PG	23.3	[28]
EDE-D301	298	[29]	DNFCs	29.6	[30]
ACWNS nodules	236.8	[31]	PN-Fe_3O_4-IDA	47.6	[32]
PCM-N	402	[33]	PBC@SiO_2-NH_2	30.0	[34]
MNP-PCP	7.48	[35]	mGO@Urea	30.7	[36]
PEI/PAN membrane	122	[37]	PEI/PAN membrane	85.1	[37]
MIL-101(Fe)@PEI	339	This study	MIL-101(Fe)@PEI	42.3	This study

pseudo-second-order kinetic model [Eq. (7)], Elovich model [Eq. (8)], double constant model [Eq. (9)] and intraparticle diffusion model [Eq. (10)] are as follows:

$$q_t = q_e\left(1 - e^{-k_1 t}\right) \tag{6}$$

$$q_t = \frac{k_2 q_e^2 t}{1 + k_2 q_e t} \tag{7}$$

$$q_t = A + B\ln t \tag{8}$$

$$\ln q_t = \ln A + K_S t \tag{9}$$

$$q_t = K_t t^{1/2} + C \tag{10}$$

where q_e (mg·g^{-1}) is the equilibrium adsorption quantity while k_1 (min^{-1}) and k_2 (mg·g^{-1}·min^{-1}) are pseudo-first-order and pseudo-second-order kinetic rate constants, respectively; K_t (mg·g^{-1}·min$^{-0.5}$) is the diffusion rate constant, and C (mg·g^{-1}) is a constant related to the thickness of the boundary layer.

The results of nonlinear regressive analysis using kinetic models are listed in Table 4. Based on values of R^2, SSE, and comparison between fitted results and experimental points, suitable model can be obtained. It was seen from Table 4a that the R^2 values obtained for all three study temperatures are greater than 0.910 while the $q_{e(\text{theo})}$ values obtained from the pseudo-second-order kinetic model are close to those of the experiments at same conditions. Furthermore, the fitting curves from

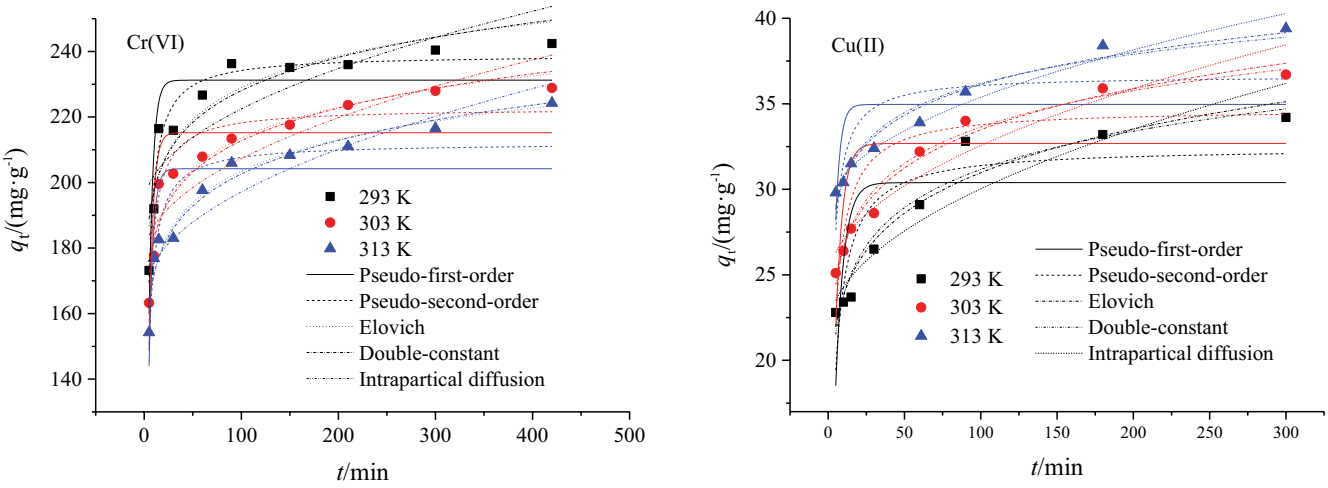

Fig. 10. Kinetic fitting curve of adsorption of Cr(VI) and Cu(II).

Table 4a
Kinetic fitting parameters of Cr(VI) adsorption by MIL-101(Fe)@PEI

Pseudo-first-order kinetic model						
T (K)	C_0 (mg·L^{-1})	$q_{e(\exp)}$ (mg·g^{-1})	$q_{e(\text{theo})}$ (mg·g^{-1})	k_1 (min^{-1})	R^2	SSE
293	300	242	232 ± 5	0.232 ± 0.032	0.703	1,350
303	300	228	221 ± 5	0.256 ± 0.037	0.748	680
313	300	224	212 ± 4	0.237 ± 0.034	0.672	1,230
Pseudo-second-order kinetic model						
T (K)	C_0 (mg·L^{-1})	$q_{e(\exp)}$ (mg·g^{-1})	$q_{e(\text{theo})}$ (mg·g^{-1})	k_2 (g·mg^{-1}·min^{-1})	R^2	SSE
293	300	242	238 ± 2	0.002 ± 2.07 × 10^{-4}	0.949	209
303	300	228	225 ± 3	0.002 ± 2.88 × 10^{-4}	0.916	313
313	300	224	215 ± 3	0.002 ± 3.98 × 10^{-4}	0.905	534
Elovich model						
T (K)	C_0 (mg·L^{-1})	A	B	R^2	SSE	
293	300	164 ± 8	14.1 ± 1.9	0.856	598	
303	300	150 ± 6	13.7 ± 1.4	0.918	216	
313	300	139 ± 4	13.8 ± 1.0	0.956	168	
Double constant model						
T (K)	C_0 (mg·L^{-1})	A	K_s	R^2	SSE	
293	300	170 ± 7	0.060 ± 0.001	0.832	692	
303	300	156 ± 5	0.060 ± 0.007	0.901	367	
313	300	145 ± 1	0.070 ± 0.005	0.947	194	
Intraparticle diffusion model						
T (K)	C_0 (mg·L^{-1})	K_t (mg·g^{-1}·min$^{-0.5}$)	C (mg·g^{-1})	R^2	SSE	
293	300	2.98 ± 0.72	192 ± 8	0.636	1,520	
303	300	3.01 ± 0.57	177 ± 7	0.588	650	
313	300	3.15 ± 0.45	165 ± 5	0.838	590	

this model are very close to the experimental points. So it is more suitable to describe the adsorption process toward Cr(VI), indicating that the adsorption process may include chemisorption.

As seen from Table 4b, the double constant model best describes the experimental data for the adsorption of Cu(II) onto MIL-101(Fe)@PEI due to the highest R^2 and lowest SSE values. Of course, the pseudo-second-order model is also suitable to describe the kinetic process of Cu(II) adsorption according to the data listed in Table 4b. Other models are not proper to predict the kinetic process.

3.2.6. Thermodynamic parameters

Thermodynamic parameters include enthalpy change ($\Delta H°$), Gibbs free energy change ($\Delta G°$) and entropy change ($\Delta S°$), which are used to describe energy change, reaction spontaneity, and the degree of randomness in the adsorption process, respectively. The above parameters can be calculated using the following equation:

$$K_c = \frac{C_{\text{ad,e}}}{C_e} \tag{11}$$

$$\Delta G° = -RT \ln K_c \tag{12}$$

$$\Delta G° = \Delta H° - T\Delta S° \tag{13}$$

where K_c is the distribution coefficient for the adsorption; $C_{\text{ad},e}$ (mg·L^{-1}) is the concentration of adsorbent on adsorbent at adsorption equilibrium; R (8.314 J·mol^{-1}·K^{-1}) is the universal gas constant and T (K) is temperature.

The activation energy (E_a) is a physical quantity related to the rate of reaction, and its value can be used to infer the speed of the adsorption process. The activation energy for Cr(VI) and Cu(II) adsorption was calculated by the Arrhenius equation (13):

$$\ln k_2 = \frac{\ln k_0 - E_a}{RT} \tag{14}$$

where k_0 (g·mg^{-1}·min^{-1}) is the temperature independent factor; E_a (kJ·mol^{-1}) is the apparent activation energy of the reaction of adsorption. When lnk_2 is plotted vs. 1/T, a straight line with slope $-E_a/R$ is obtained.

Table 4b
Kinetic fitting parameters of Cu(II) adsorption by MIL-101(Fe)@PEI

Pseudo-first-order kinetic model						
T (K)	C_0 (mg·L^{-1})	$q_{e(\text{exp})}$ (mg·g^{-1})	$q_{e(\text{theo})}$ (mg·g^{-1})	k_1 (min^{-1})	R^2	SSE
293	80	34.2	34.9 ± 1.31	0.327 ± 0.098	0.188	63.1
303	80	36.7	32.6 ± 1.51	0.222 ± 0.062	0.355	76.9
313	80	39.4	30.4 ± 1.70	0.188 ± 0.056	0.323	91.8
Pseudo-second-order kinetic model						
T (K)	C_0 (mg·L^{-1})	$q_{e(\text{exp})}$ (mg·g^{-1})	$q_{e(\text{theo})}$ (mg·g^{-1})	k_2 (g·mg^{-1}·min^{-1})	R^2	SSE
293	80	34.2	13.6 ± 1.13	0.016 ± 0.005	0.612	30.1
303	80	36.7	34.6 ± 1.19	0.011 ± 0.013	0.747	30.2
313	80	39.4	32.4 ± 1.38	0.009 ± 0.003	0.715	38.6
Elovich model						
T (K)	C_0 (mg·L^{-1})	A	B	R^2	SSE	
293	80	16.3 ± 1.23	3.22 ± 0.31	0.936	1.42	
303	80	19.4 ± 0.74	3.07 ± 0.18	0.974	0.51	
313	80	24.8 ± 0.81	2.45 ± 0.21	0.953	0.60	
Double constant model						
T (K)	C_0 (mg·L^{-1})	A	K_s	R^2	SSE	
293	80	18.2 ± 0.87	0.114 ± 0.011	0.939	1.13	
303	80	21.1 ± 0.53	0.100 ± 0.005	0.976	0.46	
313	80	25.7 ± 0.57	0.073 ± 0.005	0.968	0.41	
Intraparticle diffusion model						
T (K)	C_0 (mg·L^{-1})	K_t (mg·g^{-1}·min$^{-0.5}$)	C (mg·g^{-1})	R^2	SSE	
293	80	0.84 ± 0.12	21.6 ± 1.14	0.867	2.99	
303	80	0.81 ± 0.09	24.5 ± 0.89	0.908	1.82	
313	80	0.67 ± 0.04	28.6 ± 0.69	0.972	0.35	

The thermodynamic parameters of Cr(VI) and Cu(II) adsorption by MIL-101(Fe)@PEI are shown in Table 5. The ΔG values of the two adsorption processes in Table 5 are all less than zero, indicating that the adsorption reaction of Cr(VI) and Cu(II) by MIL-101(Fe)@PEI can occur spontaneously. The ΔG value of Cu(II) adsorption decreased from –9.84 to –11.6 kJ·mol^{-1} as the reaction temperature increased from 293 to 313 K, indicating that increasing the temperature increased the spontaneity of the adsorption reaction. The ΔH value for Cr(VI) adsorption is negative, whereas it is positive for Cu(II) adsorption. This supports the exothermic and endothermic natures of Cr(VI) and Cu(II) adsorption processes, respectively. The positive entropy (ΔS) values for both the Cr(VI) and Cu(II) adsorption processes indicate an increase in the disorderliness at the solid–liquid interface. The E_a values for the Cr(VI) and Cu(II) removal processes were 8.27 and 17.1 kJ·mol^{-1}, respectively. These small E_a values suggest the adsorption of Cr(VI) and Cu(II) was a physical process.

3.2.7. Desorption and regeneration

For practical application of MIL-101(Fe)@PEI, it is imperative to study its desorption and regeneration potentials. This will help to establish the stability, effectiveness, and reusability of the adsorbent, as well as give an indication of its cost-effectiveness [38–40].

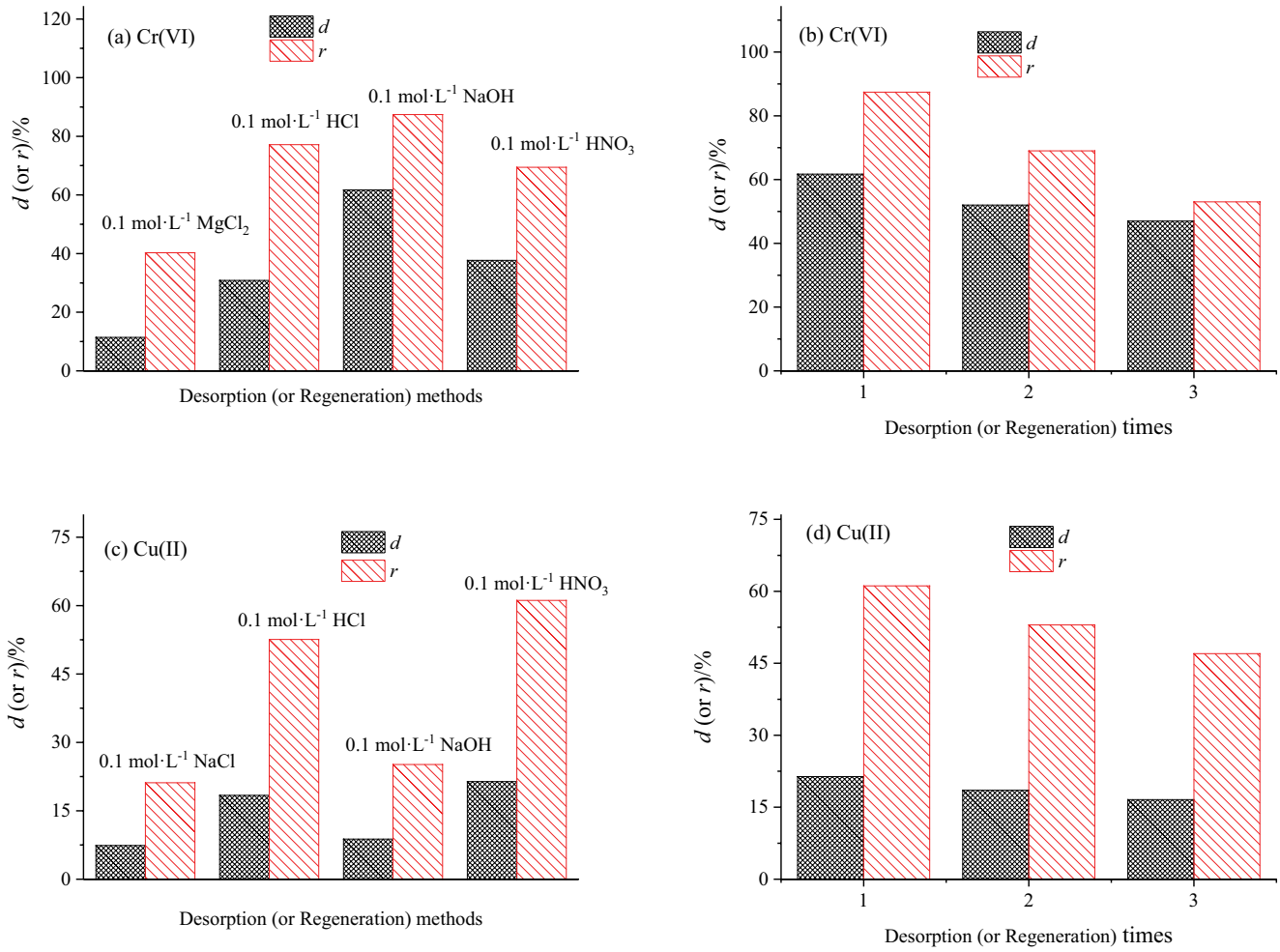

Fig. 11. Desorption and regeneration of Cr(VI) (a, b) and Cu(II) (c, d).

Table 5
Thermodynamic parameters of Cr(VI) and Cu(II) adsorption onto MIL-101(Fe)@PEI

Parameters	E_a (kJ·mol^{-1})	ΔH (kJ·mol^{-1})	ΔS (J·mol^{-1}·K^{-1})	ΔG (kJ·mol^{-1})		
				293 K	303 K	313 K
Cr(VI)	8.27	–6.1 × 10^{-3}	27.0	–4.69	–8.21	–9.84
Cu(II)	17.1	24.2	112	–2.71	–8.90	–11.6

According to the results in Fig. 11a, a 0.1 mol·L^{-1} NaOH solution achieved the highest efficiency of desorption and regeneration at 61.76% and 87.44%, respectively. This may be due to the ability of NaOH to weaken the electrostatic attraction as well as the ion exchange between the adsorbent and the Cr(VI). Subsequently, 0.1 mol·L^{-1} NaOH was used for three desorption and regeneration experiments. The desorption rate of MIL-101(Fe)@PEI decreased from 61.7% to 47.3% as the number of regenerations increased (Fig. 11b), while the regeneration rate decreased from 87.8% to 53.7%.

According to Fig. 11c, the best eluent for desorbing Cu(II) from MIL-101(Fe)@PEI was 0.1 mol·L^{-1} HNO_3. However, it recorded a relatively small efficiency of 25%. This could be due to the strong complexation forces between MIL-101(Fe)@PEI and Cu(II). Fig. 11d presents the results of three rounds of desorption and regeneration. In the third cycle, regeneration efficiency reached 50%, suggesting that the adsorbent has the potential to be reused.

3.2.8. Adsorption mechanism

The adsorption mechanism for both Cr(VI) and Cu(II) has been shown pictorially in Fig. 12. Under acidic conditions, the amino groups on the surface of MIL-101(Fe)@PEI are protonated, which is responsible for electrostatic adsorption of $HCrO_4^-$ and $Cr_2O_7^{2-}$. It is also suggested that ion exchange played an important role in the removal of Cr(VI). According to the findings, the adsorption of Cu(II) by MIL-101(Fe)@PEI was primarily mediated by surface complexation, as illustrated in Fig. 12.

3.2.9. Cost analysis

Iron is almost the cheapest metal because it is abundant in nature, easy to obtain, easy to smelt, and there is currently a great deal of iron production in the world. Comparing the cost of MIL-101(Fe)@PEI with some commercially available adsorbents and activated carbons, it is very economical to use MIL-101(Fe)@PEI. Hence, MIL-101(Fe)@PEI offers an economic advantage over commercially available adsorbents and activated carbons.

4. Conclusion

A solvothermal process was used to create a PEI functionalized MOF (MIL-101(Fe)@PEI), and the adsorption properties of MIL-101(Fe)@PEI towards Cr(VI) and Cu(II) were performed. This novel adsorbent showed superior adsorption capacity towards Cr(VI) and Cu(II) than a number of adsorbents reported in previous studies. The uptake of Cr(VI) and Cu(II) proceeded through both physical and chemical processes whereby electrostatic attraction and ion exchange accounted for the removal of Cr(VI) and surface complexation and electrostatic attraction also mediated the adsorption of Cu(II). The Freundlich isotherm model gave the best fit to equilibrium experimental data for both Cr(VI) and Cu(II) adsorption. pseudo-second-order and double constant models can be used to describe the kinetics of Cr(VI) and Cu(II) adsorption, respectively. Adsorption of Cr(VI) and Cu(II) onto MIL-101(Fe)@PEI occurs spontaneously. There is property of

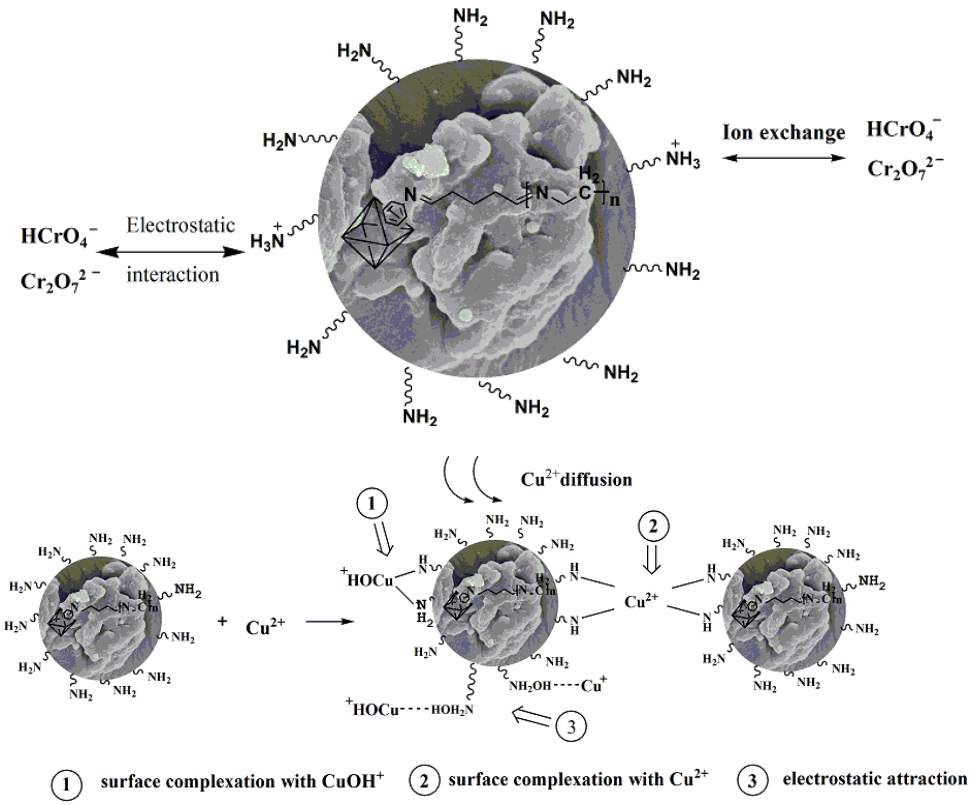

Fig. 12. Adsorption mechanism of MIL-101(Fe)@PEI for Cr(VI) and Cu(II).

regeneration and reuse for Cr or Cu loaded MIL-101(Fe)@PEI). MIL-101(Fe)@PEI as an efficient adsorbent is potential to removal of Cr(VI) and Cu(II) from solution.

Acknowledgements

This work was financially supported by the Henan Province basis and Advancing Technology Research Project (142300410224).

References

[1] K. Smith, S.M. Liu, Y. Liu, S.J. Guo, Can China reduce energy for water? a review of energy for urban water supply and wastewater treatment and suggestions for change, Renewable Sustainable Energy Rev., 91 (2018) 41–58.
[2] L.Z. Chen, F. Caro, C.J. Corbett, X.M. Ding, Estimating the environmental and economic impacts of widespread adoption of potential technology solutions to reduce water use and pollution: application to China's textile industry, Environ. Impact Assess. Rev., 79 (2019) 106293, doi: 10.1016/j.eiar.2019.106293.
[3] G.S. Yang, H.E. Lee, J.Y. Lee, Evaluation of in vitro assays for the assessment of the skin sensitization hazard of cosmetic dyes, Toxicol. Lett., 280 (2017) S268, doi: 10.1016/j.toxlet.2017.07.949.
[4] A.K. Singh, R. Chandra, Pollutants released from the pulp paper industry: aquatic toxicity and their health hazards, Aquat. Toxicol., 211 (2019) 202–216.
[5] M. Arias-Estevez, E. Lopez-Periago, E. Martinez-Carballo, J. Simal-Gandara, J.C. Mejuto, L. Garcia-Rio, The mobility and degradation of pesticides in soils and the pollution of groundwater resources, Agric. Ecosyst. Environ., 123 (2008) 247–260.
[6] J. Wojcieszek, J. Szpunar, R. Lobinski, Speciation of technologically critical elements in the environment using chromatography with element and molecule specific detection, TrAC, Trends Anal. Chem., 104 (2018) 42–53.
[7] T.L. DesMarais, M. Costa, Mechanisms of chromium-induced toxicity, Curr. Opin. Toxicol., 14 (2019) 1–7.
[8] R.A. Festa, D.J. Thiel, Copper: an essential metal in biology, Curr. Biol., 21 (2011) R877–883.
[9] V. Krstic, T. Urosevic, B. Pesovski, A review on adsorbents for treatment of water and wastewaters containing copper ions, Chem. Eng. Sci., 192 (2018) 273–287.
[10] S.F. Motevalizadeh, M. Khoobi, A. Sadighi, M. Khalilvand-Sedagheh, M. Pazhouhandeh, A. Ramazani, M.A. Faramarzi, A. Shafiee, Lipase immobilization onto polyethylenimine coated magnetic nanoparticles assisted by divalent metal chelated ions, J. Mol. Catal. B: Enzym., 120 (2015) 75–83.
[11] A.N. Kani, E. Dovi, F.M. Mpatani, A.A. Aryee, R.P. Han, Z.H. Li, L.B. Qu, A review of pollutant decontamination by polyethyleneimine engineered agricultural waste materials, Environ. Chem. Lett., 20 (2022) 705–729.
[12] A.A. Aryee, E. Dovi, Q.Y. Li, R.P. Han, Z.H. Li, L.B. Qu, Magnetic biocomposite based on peanut husk for adsorption of hexavalent chromium, Congo red and phosphate from solution: characterization, kinetics, equilibrium, mechanism and antibacterial studies, Chemosphere, 287 (2022) 132030, doi: 10.1016/j.chemosphere.2021.132030.
[13] A.N. Kani, E. Dovi, A.A. Aryee, F.M. Mpatani, R.P. Han, Z.H. Li, L.B. Qu, Polyethyleneimine modified Tiger nut residue for removal of Congo red from solution, Desal. Water Treat., 215 (2021) 209–221.
[14] H.Y. Li, S.N. Zhao, S.Q. Zang, J. Li, Functional metal–organic frameworks as effective sensors of gases and volatile compounds, Chem. Soc. Rev., 49 (2020) 6364–6401.
[15] S. Zhang, J.Q. Wang, Y. Zhang, J.Z. Ma, L.T.Y. Huang, S.J. Yu, L. Chen, G. Song, M.Q. Qiu, X.X. Wang, Applications of water-stable metal-organic frameworks in the removal of water pollutants: a review, Environ. Pollut., 291 (2021) 118076, doi: 10.1016/j.envpol.2021.118076.
[16] H.Y. Jang, J.K. Kang, J.A. Park, S.C. Lee, S.B. Kim, Metal-organic framework MIL-100(Fe) for dye removal in aqueous solutions: prediction by artificial neural network and response surface methodology modeling, Environ. Pollut., 267 (2020) 115583, doi: 10.1016/j.envpol.2020.115583.
[17] A. Hamedi, M.B. Zarandi, M.R. Nateghi, Highly efficient removal of dye pollutants by MIL-101(Fe) metal-organic framework loaded magnetic particles mediated by Poly L-Dopa, J. Environ. Chem. Eng., 7 (2019) 102882, doi: 10.1016/j.jece.2019.102882.
[18] J.M. Yang, R.Z. Zhang, Y.Y. Liu, Superior adsorptive removal of anionic dyes by MIL-101 analogues: the effect of free carboxylic acid groups in the pore channels, CrystEngComm, 21 (2019) 5824–5833.
[19] C. Arora, S. Soni, S. Sahu, J. Mittal, P. Kumar, P.K. Bajpai, Iron based metal organic framework for efficient removal of methylene blue dye from industrial waste, J. Mol. Liq., 284 (2019) 343–352.
[20] S.S. Chen, K. Wen, X.T. Zhang, R.Z. Zhang, R.P. Han, Adsorption of neutral red onto MIL-100(Fe) from solution: characterization, equilibrium, kinetics, thermodynamic and process design, Desal. Water Treat., 177 (2020) 197–208.
[21] N.C. Burtch, H. Jasuja, K.S. Walton, Water stability and adsorption in metal–organic frameworks, Chem. Rev., 114 (2014) 10575–10612.
[22] R. Liang, R. Chen, F. Jing, N. Qin, L. Wu, Multifunctional polyoxometalates encapsulated in MIL-100(Fe): highly efficient photocatalysts for selective transformation under visible light, Dalton Trans, 44 (2015) 18227–18236.
[23] A. Jarrah, S. Farhadi, Encapsulation of $K_6P_2W_{18}O_{62}$ into magnetic nanoporous Fe_3O_4/MIL-101(Fe) for highly enhanced removal of organic dyes, J. Solid State Chem., 285 (2020) 121264, doi: 10.1016/j.jssc.2020.121264.
[24] J. Yang, X. Niu, S. An, W. Chen, J. Wang, W. Liu, Facile synthesis of Bi_2MoO_6-MIL-100(Fe) metal-organic framework composites with enhanced photocatalytic performance, RSC Adv., 7 (2017) 2943–2952.
[25] H. Tian, P. Peng, Q. Du, X. Hui, H. H, One-pot sustainable synthesis of magnetic MIL-100(Fe) with novel Fe_3O_4 morphology and its application in heterogeneous degradation, Dalton Trans, 47 (2018) 3417–3424.
[26] L. Han, H. Qi, D. Zhang, G. Ye, W. Zhou, C.M. Hou, W. Xu, Y.Y. Sun, A facile and green synthesis of MIL-100(Fe) with high-yield and its catalytic performance, New J. Chem., 41 (2017) 13504–13509.
[27] L. Zhang, W.Y. Niu, J. Sun, Q. Zhou, Efficient removal of Cr(VI) from water by the uniform fiber ball loaded with polypyrrole: static adsorption, dynamic adsorption and mechanism studies, Chemosphere, 248 (2020) 126102, doi: 10.1016/j.chemosphere.2020.126102.
[28] L.N. Zhao, Q. Zhang, X.B. Li, J.J. Ye, J.Y. Chen, Adsorption of Cu(II) by phosphogypsum modified with sodium dodecyl benzene sulfonate, J. Hazard. Mater., 387 (2020) 121808, doi: 10.1016/j.jhazmat.2019.121808.
[29] S.L. Han, Y.N. Zang, Y. Gao, Q.Y. Yue, P. Zhang, W.J. Kong, Bo Jin, X. Xu, B.Y. Gao, Co-monomer polymer anion exchange resin for removing Cr(VI) contaminants: adsorption kinetics, mechanism and performance, Sci. Total Environ., 709 (2020) 136002, doi: 10.1016/j.scitotenv.2019.136002.
[30] Z.H. Lei, W.H. Gao, J.S. Zeng, B. Wang, J. Xu, The mechanism of Cu(II) adsorption onto 2,3-dialdehyde nano-fibrillated celluloses, Carbohydr. Polym., 230 (2020) 115631, doi: 10.1016/j.carbpol.2019.115631.
[31] E. Dovi, A.A. Aryee, A.N. Kani, F.M. Mpatani, J.J. Li, L.B. Qu, R.P. Han, High-capacity amino functionalized walnut shell for efficient removal of toxic hexavalent chromium ions in batch and column mode, J. Environ. Chem. Eng., 10 (2022) 107292, doi: 10.1016/j.jece.2022.107292.
[32] A.A. Aryee, F.M. Mpatani, Y. Du, A.N. Kani, E. Dovi, R. Han, Z. Li, L. Qu, Fe_3O_4 and iminodiacetic acid modified peanut husk as a novel adsorbent for the uptake of Cu(II) and Pb(II) in aqueous solution: characterization, equilibrium and kinetic study, Environ. Pollut., 268 (2021) 115729, doi: 10.1016/j.envpol.2020.115729.

[33] H.X. Liang, R.R. Sun, B. Song, Q.Q. Sun, P. Peng, D. She, Preparation of nitrogen-doped porous carbon material by a hydrothermal-activation two-step method and its high-efficiency adsorption of Cr(VI), J. Hazard. Mater., 387 (2020) 121987, doi: 10.1016/j.jhazmat.2019.121987.
[34] Y.L. Liu, J. Xu, Z. Cao, R.Q. Fu, C.C. Zhou, Z.N. Wang, X.H. Xu, Adsorption behavior and mechanism of Pb(II) and complex Cu(II) species by biowaste-derived char with amino functionalization, J. Colloid Interface Sci., 559 (2020) 215–225.
[35] A. Pholosi, E.B. Naidoo, A.E. Ofomaja, Batch and continuous flow studies of Cr(VI) adsorption from synthetic and real wastewater by magnetic pine cone composite, Chem. Eng. Res. Des., 153 (2020) 806–818.
[36] S.A. Hosseini, Z. Shokri, S. Karami, Adsorption of Cu(II) to mGO@Urea and its application for the catalytic reduction of 4-NP, J. Ind. Eng. Chem., 75 (2019) 52–60.
[37] M.Y. Liu, X.T. Zhang, R.P. Han, L.B. Qu, Crosslinked polyethylenimine/polyacrylonitrile blend membrane for multifunctional adsorption of heavy metals and endocrine disrupting chemicals in solution, J. Mol. Liq., 365 (2022) 120124, doi: 10.1016/j.molliq.2022.120124.
[38] J.L. Wang, X. Liu, M.M. Yang, H.Y. Han, S.S. Zhang, G.F. Ouyang, R.P. Han, Removal of tetracycline using modified wheat straw from solution in batch and column modes, J. Mol. Liq., 338 (2021) 116698, doi: 10.1016/j.molliq.2021.116698.
[39] S. Soni, P.K. Bajpaj, J. Mittal, C. Arora, Utilisation of cobalt doped iron based MOF for enhanced removal and recovery of methylene blue dye from wastewater, J. Mol. Liq., 314 (2020) 113642, doi: 10.1016/j.molliq.2020.113642.
[40] R.Z. Zhang, K. Wen, R.P. Han, Effective removal of phosphate from solution by iron-doped chitosan/polyvinyl alcohol composite membrane, Desal. Water Treat., 267 (2022) 98–107.